Restoring Force Model of a Cast-in-situ Recycled Aggregate Concrete Frame

Changqing Wang[1,2], Jianzhuang Xiao[1,*], Loan Pham[1] and Tao Ding[1]

[1]Department of Structural Engineering, Tongji University, Shanghai, 200092, China
[2]College of Civil Engineering and Architecture, Nanyang Normal University, Nanyang, 473000, China

(Received: 22 March 2013; Received revised form 17 November 2013; Accepted: 20 May 2014)

Abstract: The hysteresis behavior of a cast-in-situ recycled aggregate concrete (RAC) frame was analyzed based on shaking table tests on a one-fourth scaled model of a two-bay, two-span and 6-storey RAC frame. Then feature points and the stiffness degradation were defined and the deteriorating four-line-typed restoring force model was put forward. In the hysteresis model, the monotonic behavior is described by a four-line-typed skeleton curve which accounts for concrete cracking, yielding of reinforcing bars, maximum and ultimate point of the RAC frame model. The hysteresis behavior is described through a number of rules for unloading and reloading. Therefore, the restoring force model proposed in this study can capture the hysteresis response of the frame under seismic actions. Moreover, the displacement ductility of the RAC frame structure is evaluated based on the proposed restoring force model. It can be concluded from this investigation that the RAC frame structure with proper design and construction has favorable load-carrying capacity, deformation capacity, energy dissipation ability and seismic performance, and can be applied and popularized in the area with the requirement of aseismic fortification intensity.

Key words: recycled aggregate concrete (RAC), frame structure, cast-in-situ, seismic behavior, restoring force model, hysteresis rule, stiffness degradation.

1. INTRODUCTION

Study on the mechanical behavior and the seismic performance of recycled aggregate concrete (RAC) components has been performed in recent years (Xiao *et al*. 2012a). For example, the shear behavior of RAC beams (Han *et al*. 2001; Etxeberria *et al*. 2007; Fathifazl *et al*. 2010), the flexural performance of RAC beams (Fathifazl *et al*. 2009), the bearing capacity and deformability of beams and columns made of RAC (Ajdukiewicz and Kliszczewicz 2007), as well as the seismic behavior of beam-column joints made of RAC under cyclic loading (Corinaldesi and Moriconi 2006; Xiao *et al*. 2010) were investigated.

With regard to popularizing RAC, its structural behavior ought to be investigated. At present, the seismic behavior of the plane frame structure made of RAC has been investigated and discussed in some literatures. For examples, Xiao *et al*. (2006) conducted the seismic tests of four 1/2 scaled RAC frames under low-frequency cyclic lateral load with constant vertical actions and the test results revealed that the general seismic behavior of RAC frame structure declined with an increase of the recycled coarse aggregate (RCA) replacement percentage; Min *et al*. (2011) completed low-cyclic reverse lateral loading tests for two RAC frames with RCA replacements of 25% and 50% respectively, and found that the RAC frames had good seismic performance. Moreover, Cao *et al*. (2011) conducted a comparative study on the seismic behavior of two 1/2.5 scaled two-storey RAC frames under low-cyclic loading, and found that the load-carrying capacity

*Corresponding author. Email address: jzx@tongji.edu.cn; Fax: +86-21-65986345; Tel: +86-21-65982787.

of RAC frame was similar to that of conventional concrete frame. To further investigate the seismic behavior of the RAC structure, the authors of this paper finished the world's first shaking table test on a cast-in-situ RAC space frame structure and measured the dynamic characteristic and the seismic response of the RAC frame model (Xiao *et al*. 2012b), however, the restoring force model of the RAC space frame structure is not yet discussed and put forward.

In order to predict the distribution of forces and deformations in concrete structures under the maximum credible earthquake, precise models for the hysteresis behavior of the different critical regions of the structure are necessary. Several hysteresis models have been proposed and applied in past. A finite positive slope is assigned to the post-yield stiffness to account for the strain-hardening characteristic, and the model is called a bilinear model that does not represent the degradation of loading and unloading stiffness with increasing displacement amplitude reversals, and the model is not suited for a refined nonlinear analysis of a reinforced concrete structure. Likewise, a qualitative model for reinforced concrete was developed by Clough (1966) who incorporated the stiffness degradation of the elastic-plastic model, and the response waveform of the degrading stiffness model was distinctly different from that of an ordinary elastic-plastic model. The model is relatively simple, and has been applied extensively in nonlinear analysis with the inclusion of strain-hardening characteristics. A more sophisticated hysteresis model was developed by Takeda *et al*. (1970) on the basis of experimental observations. This model included stiffness changes at flexural cracking and yielding, and also strain-hardening characteristics. A model that simulates dominantly flexural stiffness characteristics was developed by Fukada (1969). The skeleton curve was a trilinear shape with stiffness changing at cracking and yielding. The degrading trilinear model can easily include strain-hardening characteristics. The hysteresis energy dissipation per cycle beyond the initial yielding is proportional to the displacement, and the equivalent viscous damping factor becomes a constant.

In this paper, based on the load-deformation curves, the pinch behavior, the stiffness degradation and the energy dissipation of the RAC frame structure are intensively analyzed and discussed. The deteriorating four-line-typed restoring force model is proposed based on the calculation and analysis of hysteresis curves, skeleton curve and characteristic parameters of the tested cast-in-situ RAC frame model. The ductility ratio is also analyzed and discussed.

2. RESEARCH SIGNIFICANCE

Based on the finished shaking table tests of RAC frame model performed on a shaking table under a series of base excitations with gradually increasing acceleration amplitudes, the seismic behavior of the RAC frame structure was experimentally investigated, and the restoring force model of the RAC frame structure is also proposed. The study attempts to provide much deep insight into the overall dynamic behavior of the structural system and accumulates the experimental evidence for establishing related design guidelines for such RAC frame structure in the earthquake areas. Moreover, the test results may provide some technical supports for the popularization and application of the structural RAC.

3. RAC FRAME MODEL AND SHAKE TABLE TEST

3.1. Description of the Frame Model

The RAC frame model is a 2-bay, 2-span and 6-storey frame structure regular in elevation. The plane dimensions of the frame are 2175 mm × 2550 mm, and the height of each story is 750 mm. The column sections are 100 mm×100 mm, and the beam sections are 62.5 mm×125 mm in the X direction, and 50 mm×112.5 mm in the Y direction, respectively. The thickness of the slab is 30 mm. The details of the general geometry, the element sections, corresponding reinforcements of the RAC frame model and the beam-column joint details are shown in Figure 1. An additional mass of 1528 kg was attached to each slab from the 1st to the 5th floor and 1375 kg to the roof floor in order to simulate the mass density of material and loading conditions.

Ordinary Portland cement with a 28 day nominal compressive strength grade of 42.5 MPa was used in the investigation. The fine aggregate was river sand with particle diameter of 0–5 mm. The applied coarse aggregate was RCA with particle diameter of 5–10 mm, and more detailed information on the physical properties of the RCA is listed in Table 1. The recycled concrete mixture of nominal strength grade C30 was proportioned with the RCA replacement percentage equal to 100%. Because the water absorption of RCAs is greater than that of natural coarse aggregates (NCAs), the additional water should be considered in the mix proportion design of RAC, and the mix proportion used in this study was water: cement: sand: RCA = 1:1.887:2.301:3.312. The detailed information on the material properties of the RAC is presented in the reference (Xiao *et al*. 2012b; Liu *et al*. 2011). According to the Chinese Building Standard GB 50010 (2010) and similitude laws of the frame model, galvanized fine iron wires were used to model rebars. Fine iron wires of 8# and 10# were adopted as the

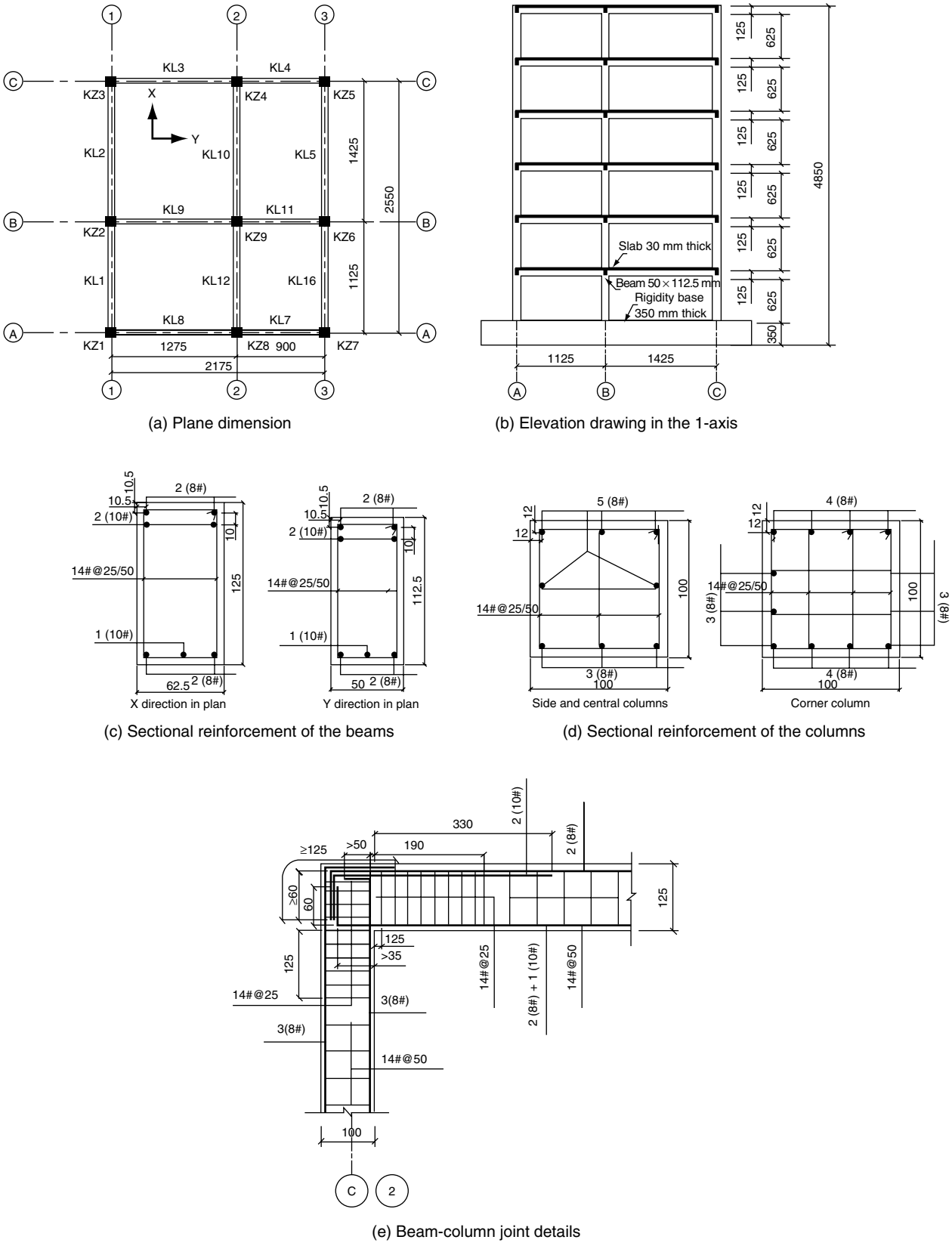

(a) Plane dimension

(b) Elevation drawing in the 1-axis

(c) Sectional reinforcement of the beams

(d) Sectional reinforcement of the columns

(e) Beam-column joint details

Figure 1. Configuration and reinforcement of space frame specimens (Unit: mm)

longitudinal rebars and 14# for stirrups in the investigation (Xiao *et al*. 2012b). An overview of the test model is shown in Figure 2.

3.2. Summary of the Shake Table Test

The displacement and acceleration, the crack development, and the plastic hinge development of each

Table 1. Physical properties of RCA

Grading (mm)	Apparent density (kg/m^3)	Water absorption (%)	Crushing value (%)
5-10	2520	11.555	15.2

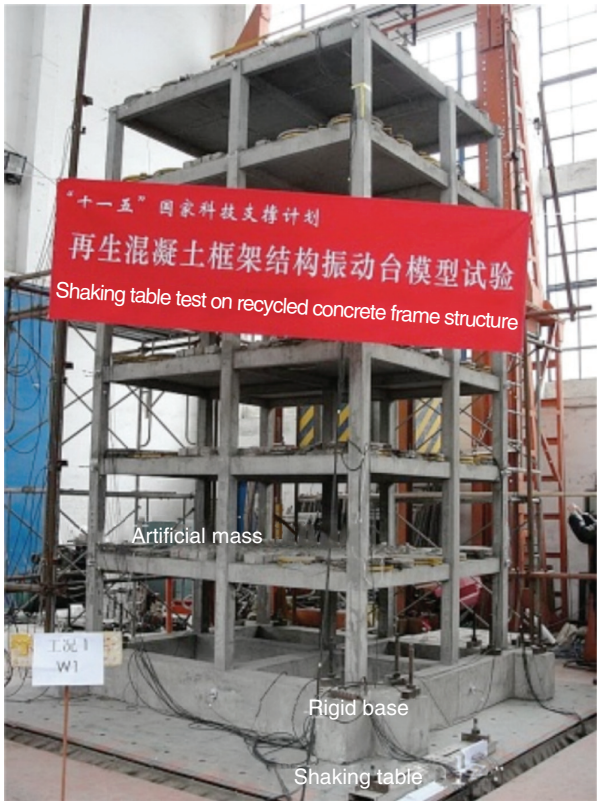

Figure 2. General view of the RAC space frame model

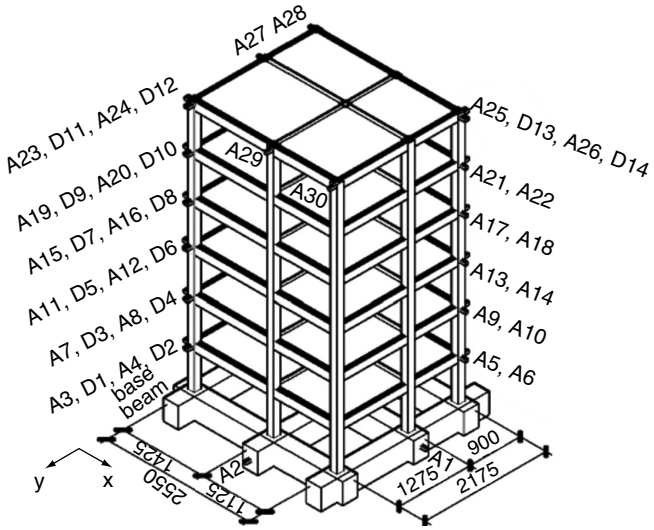

Figure 3. Arrangement of accelerometers and displacement LVDTs (Unit:mm)

element were mainly observed and measured. As illustrated in Figure 3, there were a total of 30 accelerometers installed with 1 accelerometer on the top of base on both X- and Y- directions, 4 accelerometers on each floor from the 1st to the 5th, 8 accelerometers on the roof. A total of 14 displacement Linear Variable Differential Transducers (LVDTs) were installed with 1 displacement LVDT on each floor from the 1st to the 5th in both X- and Y- directions, 4 displacement LVDTs on the roof. Other detailed information and scaling parameters can be found in the reference (Xiao *et al.* 2012b).

According to the Code for Seismic Design of Buildings (GB 50011 2010), the Wenchuan earthquake record of acceleration (WCW) which was observed at AnXian Tashui seismostation in Sichuan (2008), the EL Centro earthquake record of acceleration (ELW) (1940) and the Shanghai artificial wave (SHW) were selected as input excitations. The test program consisted of nine phases, which are tests with peak ground acceleration (PGA) of 0.066 g, 0.130 g (frequently occurring earthquake of intensity 8), 0.185 g, 0.264 g, 0.370 g (basic occurring earthquake of intensity 8), 0.415 g, 0.550 g, 0.750 g (rarely occurring earthquake of intensity 8), and 1.170 g (rarely occurring earthquake of intensity 9).

Before and after each test phase, white noise with acceleration amplitude of 0.05 g was input to check the dynamic characteristics of the model. WCW, ELW and SHW were input in sequence to the model in each test phase. The tests were performed with the main excitation in the X-direction. Among the three earthquake waves, dynamic response caused by SHW was the largest, followed by WCW and ELW (Xiao *et al.* 2012b), respectively.

4. MAIN TEST RESULTS

4.1. Typical Test Failure Pattern

During the test with PGA of 0.066 g, no visible cracks appeared on the model, it can be suggested that the model remained in the elastic stage. Under the test phase with a PGA of 0.130 g, although no visible cracks were found, combined with the analysis of structural dynamic characteristics (see Table 2), it can be inferred that the model structure stepped into the non-linear elastic stage.

Table 2. The first natural frequency (Hz) in the X-and Y-direction

		PGA (g)					
Wave	**Direction**	**Initial**	**0.066**	**0.130**	**0.370**	**0.750**	**1.170**
White noise	X	3.715	3.715	2.654	1.725	1.061	0.796
	Y	3.450	3.450	3.184	2.654	1.858	1.858
WCW	X	—	3.715	2.919	1.990	1.194	0.929
ELW	X	—	3.715	2.919	1.858	1.194	0.796
SHW	X	—	3.715	2.654	1.725	1.061	—

After the test with a PGA of 0.750 g, the RAC frame structure model was subjected to obvious damage, which includes: (1) several new minor cracks emerged at the top of the 2nd floor column KZ1 and the bottom of the third floor column KZ2; (2) the vertical cracks found first in the previous test phases extended further at the left end of the beam KL6 ranged from the 1st to the 3rd floor with the crack width of about 2 mm; (3) several new slight cracks emerged at the ends of the column KZ6 ranged from the second to the third floor.

The test with a PGA of 1.170 g caused serious damage to the model. Major cracks spread at the ends of beams KL1, KL2, KL5 and KL6 from the 1st to the 3rd floor. Fine cracks occurred horizontally on the bottom of column KZ1, KZ2, KZ3, KZ5, KZ6 and KZ7 at the 1st floor, and on the bottom of column KZ2 at the 2nd floor. The typical failure pattern can be seen in Figure 4.

4.2. Hysteresis Curves

Structures subjected to an earthquake ground motion are expected to dissipate energy, which reduces the amplitude of vibration conversely until the final stationary state is reached. The dissipating energy mainly loses through inelastic cyclic response and internal friction. Consequently, as soon as deformations reach the range of inelastic behavior, damage occurs. The relationship between restoring force and relative displacement in a loading-unloading cycle in the range of inelastic behavior is defined as hysteresis curve. It reflects the deformation characteristics, the stiffness degradation and the energy dissipation of the structure in the earthquake loading process, and provides the basis for determining the restoring force model and performing the nonlinear earthquake response analysis. Because the first and second floors are weak stories of

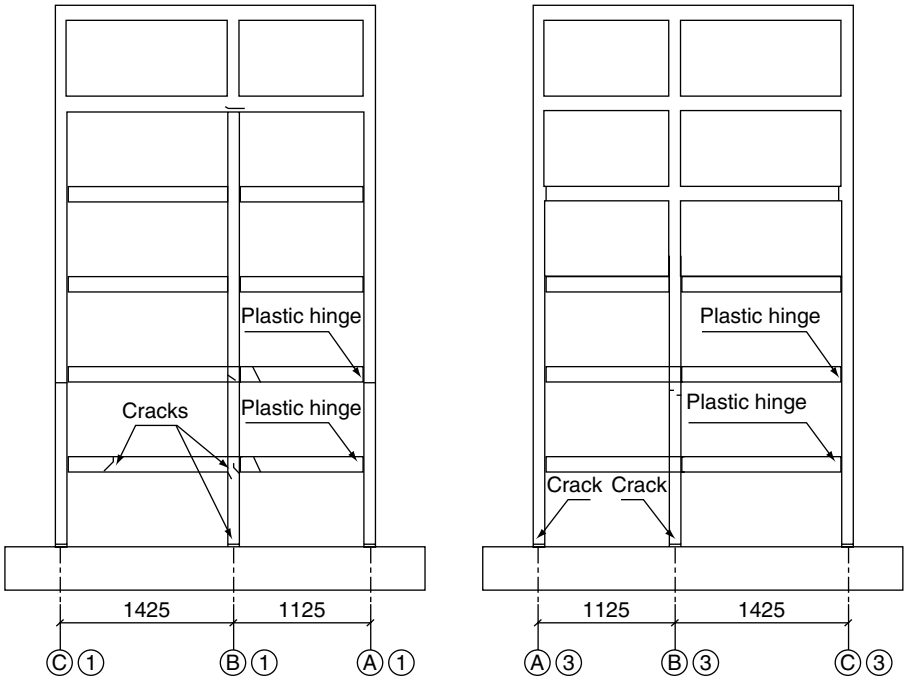

Figure 4. Failure pattern of the tested model (Unit:mm)

the frame structure, the base shear-the roof displacement relation curves, the inter-storey shear-the inter-storey drift relation curves of the first floor, and the inter-storey shear-the inter-storey drift relation curves of the second floor obtained from SHW are plotted and analyzed in Figures 5 to 7, respectively. As shown in Figures 5 to 7, it is evident that before initial cracking of the RAC frame model, the force-displacement relation curves of the structure are of straight line basically. It is therefore indicated that the structure remains in the elastic state. After cracks appeared in the model, the hysteresis loop area is very small at first. However, with the structural cracks developing gradually, the hysteresis curves pinch progressively and resemble a crescent moon shape, which means that no obvious shear deformation and slippage occur. With increasing input acceleration amplitudes, the hysteresis loops

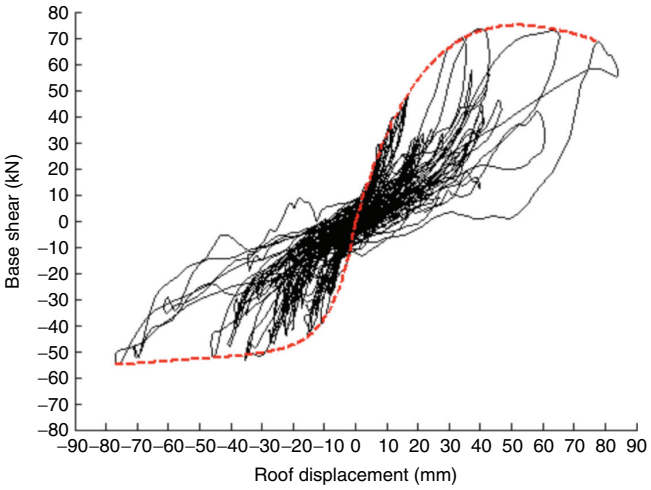

Figure 5. Restoring force curves of the roof

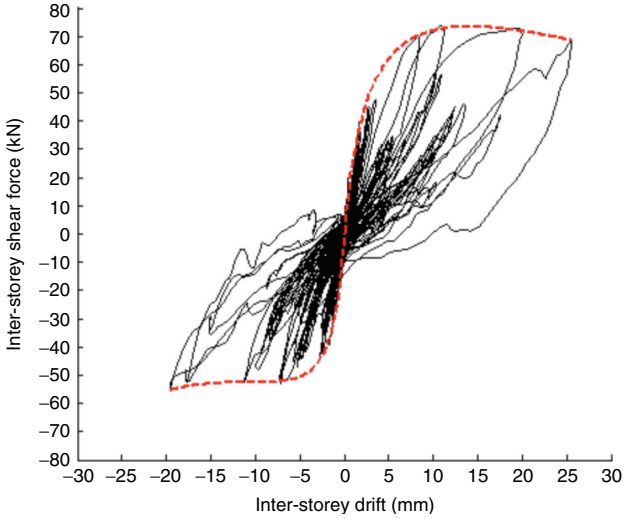

Figure 6. Inter-storey restoring force curves of the first floor

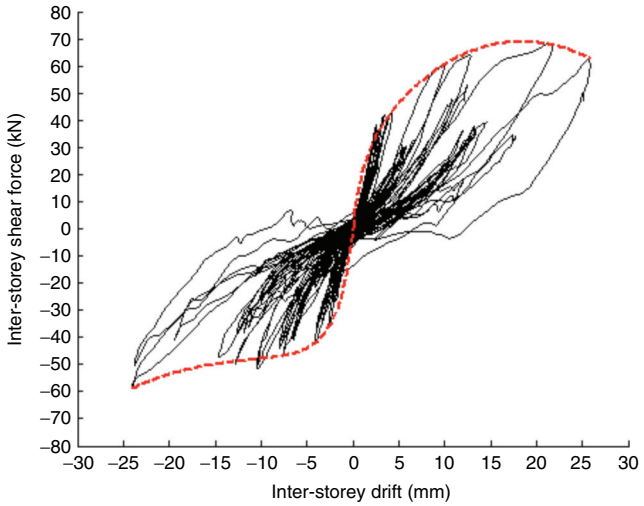

Figure 7. Inter-storey restoring force curves of the second floor

plump and pinch significantly near the origin of the coordinates, and the hysteresis curves show a reversed *S* shape, because of the shear deformation and decline in hysteresis curves. With development of concrete cracking and non-elastic deformation of the structure progressively, the lateral stiffness, the loading and the energy dissipation capacity of the structure degrade gradually, and the pinch effect of the hysteresis loops are more obvious. Analysis results demonstrate that the hysteresis behavior of the RAC frame structure is similar with that of the natural aggregate concrete (NAC) frame structure (Joseph *et al*. 1995; Lu *et al*. 2008; Xiao *et al*. 2011; Liu *et al*. 2002).

4.3. Skeleton Curves

The peak base shear force and the corresponding roof displacement in each successive test phase are given in

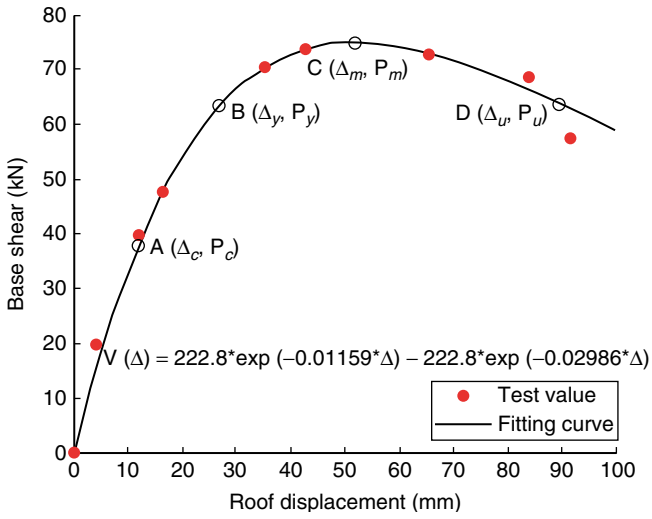

Figure 8. Overall skeleton curve of the RAC frame model

Figure 8. Based on MATLAB curve fitting toolbox, an exponential function model is adopted to represent the experimentally measured data points. The overall skeleton fitting curve is plotted against these data points in Figure 8, and the corresponding fitting formula is expressed as follows:

$$V(\Delta) = 222.8 \times \left[e^{(-0.01159\Delta)} - e^{(-0.02986\Delta)} \right] \quad (1)$$

where V is the base shear (kN), and Δ is the roof displacement (mm).

It is noticed that the relationship between the base shear and the roof displacement is expressed under the test phases with PGAs from 0.066 g to 1.170 g. Here, the value range of the independent variable Δ is from 0 mm to 100 mm in Eqn 1. From the skeleton fitting curve, the cracking loading point, the yield loading point, the maximum loading point as well as the ultimate loading point can be easily recognized. Generally, the skeleton curve can reflect the variation of the lateral loading capacity of the structure, and the slope of the curve represents the overall lateral stiffness of the structure.

The overall skeleton curve of the RAC frame model as shown in Figure 8 is analyzed, and the main seismic behavior of the RAC frame model can be summarized as follows:

- Under the test phase with a PGA of 0.066 g, the maximum displacement of the roof is 4.144 mm in the X direction, and the maximum base shear force is 26.67% of the maximum base shear bearing capacity, which proves that the tested model structure remains in the elastic state.
- Under the test phase with a PGA of 0.130 g, the maximum displacement of the roof is 11.887 mm in the X direction, and the maximum base shear force is 53.33% of the maximum base shear bearing capacity, which proves that the tested model structure steps into the elastic-plastic stage.
- Under the test phases with PGAs from 0.185 g to 0.370 g, the maximum displacement of the roof in the X direction ranges from 16.697 mm to 35.268 mm, and the corresponding maximum base shear force is about from 63.99% to 94.61% of the maximum base shear bearing capacity. It can be inferred that the structural loading capacity and the structural lateral stiffness degrades significantly, and the elastic-plastic deformation of the structure further develops.
- Under the test phase with a PGA of 0.415 g, the maximum displacement of the roof is 42.900 mm in the X direction, and the base shear force is about 99.06% of the maximum base shear bearing capacity. That is, the base shear force is approximately equal to the maximum bearing capacity value.
- Under the test phase with a PGA of 0.550 g, the maximum displacement of the roof is 65.509 mm in the X direction, and the maximum base shear force is approximately 97.91% of the maximum base shear bearing capacity. It can be found that the roof displacement increases substantially.
- Under the test phase with a PGA of 0.750 g, the maximum displacement of the roof in the X direction is 83.929 mm, and the maximum base shear force is about 92.08% of the maximum base shear bearing capacity.
- The maximum roof displacement is about 92 mm in direction X, and the maximum base shear force is about 88.69% of the maximum base shear bearing capacity after the test phase with a PGA of 1.170 g. In general, the failure load of the structure is approximately 85% of the maximum bearing capacity, it can be inferred that the RAC frame model structure underwent serious damages during this earthquake test. However, the RAC frame model structure did not collapse after all test runs.

The initial cracking point A, the yield point B, the maximum load point C, and the ultimate load D are the key points of the skeleton fitting curve as shown in Figure 8. Likewise, the corresponding loads and displacements of the characteristic points are expressed as: the cracking load P_c and the cracking displacement Δ_c; the yield load P_y and the yield displacement Δ_y; the maximum load Δ_m and the corresponding displacement Δ_m; the ultimate load P_u, and the ultimate displacement Δ_u. The experimental characteristic values of the skeleton fitting curves of the model under earthquake tests are presented in Table 3, and the normalized characteristic values of each key point are list in Table 4.

The initial crack is defined as the point where the first group of obvious cracks formed on the frame structure. The value of this point can be determined by the corresponding test data at the first crack point where the curve makes a turning, and the initial crack occurs on the model in the 0.130 g test phase in this study. At the point of maximum load, the deformation increased rapidly while the load began to descend. Generally the ultimate load is defined as the maximum load descended to about 85% and the corresponding deformation is the ultimate deformation. In fact no clear yield point was obtained from the tested model during the earthquake testing. In order to discuss the deformation

Table 3. Load and displacement of the feature points

Feature point parameters		Overall skeleton	Inter-storey skeleton curve for the 1st floor	Inter-storey skeleton curve for the 2nd floor
Feature load (kN)	P_c	37.890	28.857	37.815
	P_y	63.416	59.981	60.050
	P_m	74.788	74.456	74.456
	P_u	63.569	66.250	63.287
Feature displacement (mm)	Δ_c	11.890	1.850	2.680
	Δ_y	26.974	6.012	6.0275
	Δ_m	52.000	14.883	14.925
	Δ_u	89.502	25.660	27.914
Ductility factor	u	3.318	4.268	4.631

Table 4. Normalized feature parameters

Feature parameters	Overall skeleton	Inter-storey skeleton curve for the 1st floor	Inter-storey skeleton curve for the 2nd floor
P_m	1.000	1.000	1.000
P_u	0.850	0.890	0.850
P_y	0.848	0.806	0.807
P_c	0.507	0.388	0.508
Δ_u	1.000	1.000	1.000
Δ_m	0.581	0.580	0.535
Δ_y	0.301	0.234	0.216
Δ_c	0.133	0.072	0.096

appropriately, the equivalent yield point must be rationally determined. The general yield moment method is used to analyze the skeleton curve of the RAC frame model. As shown in Figure 9, K_0 is the initial tangent stiffness of the skeleton curve, and the point m is the maximum load point on the skeleton curve. The line OA intersects the line AC at A, from the point A to draw the vertical line which intersects the skeleton at B, to draw the line OB and extend it to get the intersecting point C, from the point C to draw the vertical line which intersects the skeleton at Y. With this method, the equivalent yield point Y required is determined on the skeleton curve.

Similarly, in this study, the inter-storey skeleton fitting curves for the 1st floor and the 2nd floor are also presented as illustrated in Figure 10 and Figure 11, and the corresponding fitting formula is expressed as follows:

$$V(\Delta_i)=\frac{-769.5\Delta_i^2+50550\Delta_i+110.5}{\Delta_i^2+341.1\Delta_i+2514}-0.044 \qquad (2)$$

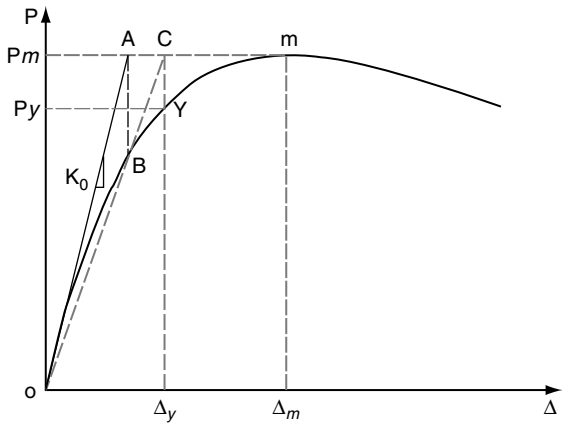

Figure 9. Definition of the yield point

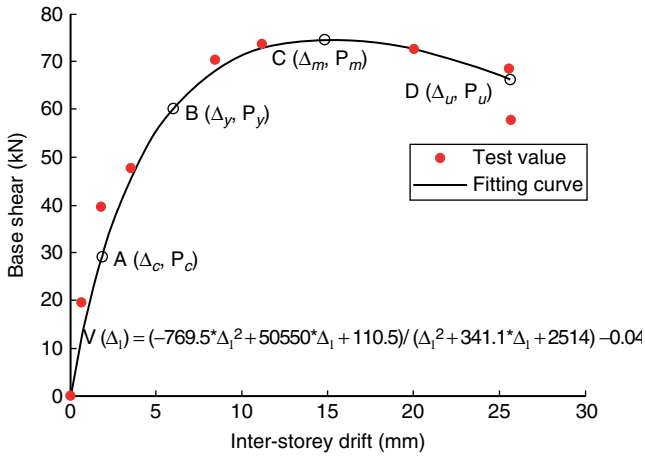

Figure 10. Inter-storey skeleton curve of the 1st floor

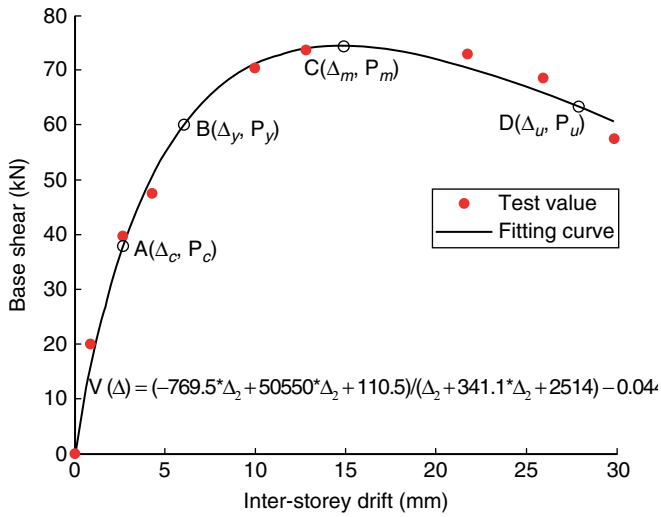

Figure 11. Inter-storey skeleton curve of the 2nd floor

where V is the base shear (kN), and Δ_i is inter-storey drift of the i^{th} floor.

The relationship between the base shear and the inter-storey drift for the weak stories is expressed under the test phases with the peak ground accelerations from 0.066 g to 1.170 g. Here, the value range of the independent variable Δ_i is from 0 mm to 30 mm in Eqn 2. Test results given by Xiao *et al*. (2012b) show that the RAC frame model has obvious weak stories, which are the first storey and the second storey of the structure that suffered more serious damage than other floors. Therefore, in this study, the hysteresis behavior of the 1st and 2nd floor is only investigated and discussed, and the load and displacement of the feature points as well as the normalized feature parameters of the inter-storey skeleton fitting curves for them are also given in Table 3 and Table 4, respectively.

According to the load and displacement of the feature points as presented in Table 3, the loading stiffness of the tested model has been calculated as listed in Table 5. As presented in Table 5, the stiffness before cracking is K_1, the stiffness after cracking is $K_2=\beta_1 K_1$, the stiffness after yielding is $K_3=\beta_2 K_1$, and the stiffness after the maximum loading is $K_4=\beta_3 K_1$.

4.4. Displacement Ductility Evaluation of the RAC Frame Model

A ductility ratio is defined in this study to evaluate the ductility of the RAC frame model, and the formula to calculate the ductility factor is expressed in Eqn 3 as follows:

$$\mu = \frac{\Delta_u}{\Delta_y} \tag{3}$$

where, μ is the ductility ratio, Δ_y and Δ_u are defined as shown in skeleton curves. Because the descending branch of the inter-storey skeleton curve for the first floor did not falls below 0.85 P_m, the ductility factor (μ) is calculated based on the maximum inter-storey drift.

The average displacement ductility ratio obtained from the overall skeleton fitting curve not the measured curve (Xiao *et al*. 2012b) and the inter-storey skeleton fitting curves of the 1st and 2nd floor are 3.318, 4.268 and 4.631, respectively, as listed in Table 3. The displacement ductility ratios show that the RAC frame model structure is properly designed and meets the structural seismic requirements of the Chinese code (GB 50011 2010). Many related experimental investigations and theoretical analysis show that the displacement ductility ratio of the concrete structures is generally between 3 to 5 (Park and Paulay 1975). It is revealed that the RAC structure and the NAC structure have very similar displacement ductility and deformation capacity. The failure mode of the RAC frame model is of typical 'strong column and weak beam'. The rational designed RAC frame model structure can be controlled within the allowable deformability, and it is able to withstand a rarely occurring earthquake of intensity 8. The rational design here referred to a rational shear coefficient as given by Xiao *et al*. (2012b) and arrangement of the reinforcement of the frame beams and columns. So as to form rational failure mechanism of the structure, the tested model failed in the following order: firstly, some slight curved cracks emerged at the ends of some frame beams ranging from the first to second floor during the test phases with PGAs from 0.185 g to 0.550 g;

Table 5. Loading stiffness

Stiffness	K_1 (kN/mm)	K_2 (kN/mm)	K_3 (kN/mm)	K_4 (kN/mm)	β_1	β_2	β_3
Overall skeleton	3.187	1.692	0.4544	-0.2992	0.531	0.143	-0.094
Inter-storey skeleton curve for the 1st floor	15.598	7.478	1.6317	-0.7614	0.4794	0.1046	-0.088
Inter-storey skeleton curve for the 2nd floor	14.110	6.642	1.6191	-0.8599	0.4707	0.1147	-0.0609

secondly, the vertical cracks extended further at the ends of the beams ranging from the first to third floor, and several new fine cracks emerged at the top of the second floor column KZ1 and the bottom of the third floor column KZ2 in the 0.750 test phase; major cracks spreaded to form plastic hinge at the ends of the beams ranging from the first floor to the third floor, and fine cracks occurred horizontally on the bottom of the columns at the first floor in the 1.170 g test phase.

5. RESTORING FORCE MODEL

5.1. Restoring Force Characteristic Skeleton Curve

In this study, for the tested model a gradual failure process is designed and the test procedure is used to demonstrate the design principle of energy dissipation. Combined the skeleton curves and the stiffness degradation of the RAC frame model, and based on results from a substantial amount of experimental test data on the tested RAC frame model, a deteriorating four-line-typed restoring force model is put forward for the RAC frame structure in this paper as shown in Figure 12. The unique restoring force model skeleton curve consisting of four linear segments with a negative stiffness for the last segment is determined by four pairs of values of lateral load and displacement (P_c, Δ_c; P_y, Δ_y; P_m, Δ_m and P_u, Δ_u), which defines characteristics corresponding to the cracking point, the yielding point, the maximum load point, and the ultimate load point of the behavior of the RAC frame model, respectively. The cracking point represents where a major crack appears, the yielding point is identified by the reinforcement at the yielding, the maximum load point represents where the base shear force reaches the maximum value, and the ultimate load point is identified by the limited value of the inter-story drift ratio. Compared with the Tomazevic and Lutman's restoring force model (Tomazevic et al. 1996a, b), the deteriorating four-line-typed restoring force model in the present study has an additional yield point. This model takes fully into account the stiffness changes at cracking, yielding, and maximum load point, as well as the strain-hardening characteristics.

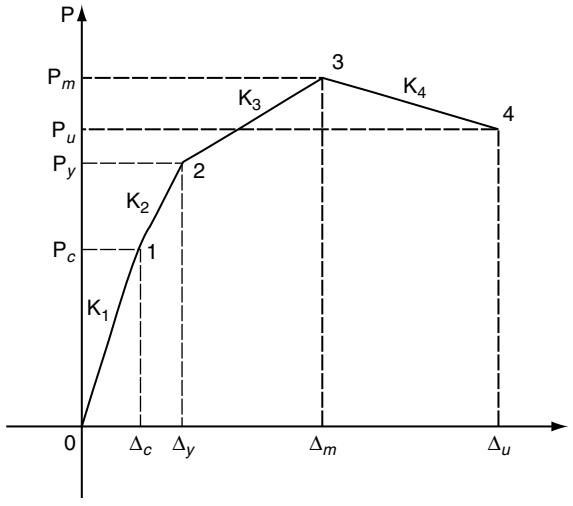

Figure 12. Restoring force model skeleton curve of the RAC frame

5.2. Feature Point Parameters Determination

The shear capacity, maximum load P_m is determined according to the following Eqn 4.

$$P_i(t) = \sum_{j=i}^{n} F_j(t) = -\sum_{j=i}^{n} m_j \left\{ \ddot{u}_j(t) + \ddot{u}_g(t) \right\} \tag{4}$$

where $P_i(t)$ (N) is the story shear of the floor j at the time of t, $F_j(t)$ (N) denotes seismic force of the floor j at the time of t, m (kg) is the lumped mass (Zhang 2001) of the floor j, $\ddot{u}_j(t) + \ddot{u}_g(t)$(g) means the absolute acceleration response of the floor j at the time of t, and n represents the total number of floors of the structure.

According to the test results as listed in Table 4, the initial cracking load of the RAC frame model is calculated by the following formula:

$$P_c = 0.51 P_m \tag{5}$$

The yield load is determined by the general yield moment method which is mentioned in the above section 4.3 and illustrated in Figure 9.

The ultimate load is calculated using the following formula according to Table 4:

$$P_u = 0.85 P_m \tag{6}$$

The cracking displacement is calculated by Eqn 7 as follows:

$$\Delta_c = \frac{P_c}{K_1} \tag{7}$$

The calculation formula of the yield displacement is listed and expressed as follows:

$$\Delta_y = \frac{P_y - P_c}{K_2} + \Delta_c \tag{8}$$

The displacement at the maximum load is calculated using Eqn 9 as follows:

$$\Delta_m = \frac{P_m - P_y}{K_3} + \Delta_y \tag{9}$$

The calculation formula of the ultimate displacement is introduced and expressed as follows:

$$\Delta_u = \frac{P_u - P_m}{K_4} + \Delta_m \tag{10}$$

where K_1, K_2, K_3 and K_4 are determined according to Table 5.

5.3. Loading Stiffness

The transformation rule on the loading stiffness is illustrated in Figure 12. The elastic stage (0–1) corresponds to the elastic stiffness K_1, the elastic-plastic stage (1–2) corresponds to the pre-yield stiffness K_2, the elastic-plastic stage (2–3) corresponds to the post-yield stiffness K_3, the failure stage (3–4) corresponds to the negative stiffness K_4. The initial stiffness K_1 can be determined in accordance with the test results and statistical data, and the stiffness of every stage can adopt the recommendation in Table 5. The initial crack point, yield point, maximum load point, ultimate load point were determined respectively according to the preceding definition and statistical data.

5.4. Unloading Stiffness

The degrading rule of stiffness is mainly related to the unloading stiffness displayed in Figure 13. Based on the normal hysteresis loops obtained from the statistical data at the cracking point, the yield point, the maximum point and the ultimate load point, the unloading stiffness of the RAC frame model at three stages is constructed. To calculate the described conditions the following calculation formulas of the unloading stiffness at three stages are considered.

In the elastic-plastic stage (1–2), the unloading stiffness K_{u1} is expressed as follows:

$$K_{u1} = K_1 = \frac{P_c}{\Delta_c} \tag{11}$$

In the elastic-plastic stage (2–3), the unloading stiffness K_{u2} is introduced and expressed as follows:

$$K_{u2} = K_{12} = \frac{P_y}{\Delta_y} \tag{12}$$

In the failure stage (3–4), the unloading stiffness K_{u3} is described and expressed as follows:

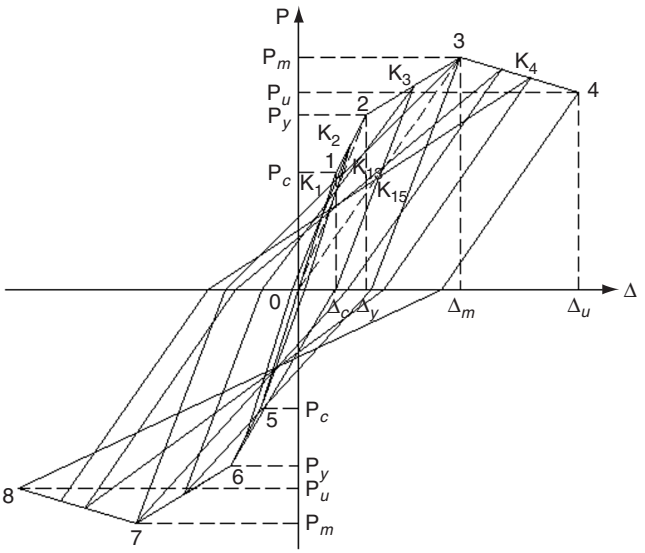

Figure 13. Define hysteresis rules of the restoring forcing model

$$K_{u3} = K_{13} = \frac{P_m}{\Delta_m} \tag{13}$$

5.5. Hysteresis Rules of the Restoring Forcing Model

To describe the hysteresis behavior of the RAC frame model, a hysteresis rule is needed. The first hysteresis law was proposed by Clough (1966). A more refined hysteresis model was proposed by Takeda *et al*. (1970). In the authors' model the monotonic behavior is described by a four-line-typed skeleton curve which accounts for cracking of concrete, yielding of reinforcing steel, maximum loading point and ultimate loading point of the RAC frame model. The hysteresis behavior is described through a number of rules for unloading and reloading and is based on experimental data obtained from the tested model during earthquake test runs. The following typical rules as shown in Figure 13 define the hysteresis behavior:

- Segment 0–1 (in positive direction) or segment 0-5 (in negative direction) as the first segment of the four-line-typed skeleton curve represents the stage of the structure, and is determined by a pair of values of lateral load and displacement (P_c, Δ_c), which defines characteristics corresponding to the cracking point (1 or 5) of the RAC frame model. In this stage, the loading stiffness is K_2 determined by Table 5, the stiffness degradation and residual displacement are not considered, and the stiffness degradation factor β is equal to 1.0.

- Segment 1–2 (in positive direction) or segment 5–6 (in negative direction) as the second segment of the four-line-typed skeleton curve represents post-cracking stage of the structure, and is determined by two pairs of values of lateral load and displacement (P_c, Δ_c; P_y, Δ_y), which define characteristics corresponding to the cracking point (1 or 5) and the yielding point (2 or 6) of the RAC frame model. The loading stiffness of the stage is K_2 determined by Table 5, the stiffness degradation and residual displacement are considered, and the stiffness degradation factor β is equal to K_2/K_1 as presented in Table 5 in this elastic-plastic stage. The unloading stiffness of the stage is K_1, the stiffness degradation and residual displacement are not considered, and the stiffness degradation factor α is equal to 1.0 in this elastic-plastic stage. In this stage, after unloading to the zero load point, the first unloading path (negative loading path) is aimed at point 5, defining the crack limit state, and the subsequent negative loading curve is aimed at the maximum point of segment 5–6.
- Segment 2–3 (in positive direction) or segment 6–7 (in negative direction) as the third segment of the four-line-typed skeleton curve represents post-yielding stage of the structure, and is determined by two pairs of values of lateral load and displacement (P_y, Δ_y; P_m, Δ_m), which define characteristics corresponding to the yielding point (2 or 6) and the maximum load point (3 or 7) of the RAC frame model. The loading stiffness of the stage is K_3 determined by Table 5, the stiffness degradation and residual displacement are considered, and the stiffness degradation factor β is equal to K_3/K_1 as presented in Table 5 in this elastic-plastic stage. The unloading stiffness of the stage is K_{u2} determined by Eqn 12, the stiffness degradation and residual displacement are considered, and the stiffness degradation factor β is equal to K_{u2}/K_1 in this elastic-plastic stage. In this stage, after unloading to the zero load point, the first unloading path (negative loading path) is aimed at point 6, defining the yield limit state, and the subsequent negative loading curve is aimed at the maximum point of segment 6–7.
- Segment 3–4 (in positive direction) or segment 7–8 (in negative direction) as the fourth segment of the four-line-typed skeleton curve represents failure stage of the structure, and is determined by two pairs of values of lateral load and displacement (P_m, Δ_m; P_u, Δ_u), which define characteristics corresponding to the maximum load point (3 or 7) and the ultimate load point (4 or 8) of the RAC frame model. The loading stiffness of the stage is K_4 determined by Table 5, the stiffness degradation and residual displacement are considered, and the stiffness degradation factor β is equal to K_4/K_1 as presented in Table 5 in this ultimate limit stage. The unloading stiffness of the stage is K_{u3} determined by Eqn 13, the stiffness degradation and residual displacement are considered, and the stiffness degradation factor β is equal to K_{u3}/K_1 in this ultimate limit stage. In this stage, after unloading to the zero load point, the first unloading path (negative loading path) is aimed at point 7, defining the ultimate limit state, and the subsequent negative loading curve is aimed at the maximum point of segment 7–8.

The feature point parameters of the deteriorating four-line-typed restoring force model are obtained from the overall skeleton curve (Figure 8), and the inter-storey skeleton curves (Figures 10 and 11) which are derived from the tested hysteresis curves of the RAC frame structure (Figures 5 to 7). Therefore, the deteriorating four-line-typed restoring force model captures the hysteresis behavior of the structure at different nonlinear stages.

5.6. Stiffness Degradation

Stiffness degradation occurred when the tested model was subjected to a series of simulated seismic ground motions with an increasing intensity of shaking. Based on the base shear, the roof displacement as well as the inter-storey drift of the RAC frame model, the overall converted stiffness and the inter-storey converted stiffness can be determined, and the converted stiffness calculation formulas are defined and expressed in Eqns 14 and 15, respectively:

$$K = \frac{V}{\Delta} \tag{14}$$

$$K_i = \frac{V}{\Delta_i} \tag{15}$$

where K is the overall converted stiffness, and K_i is the inter-storey converted stiffness; V is the total base shear;

Δ is the roof displacement, and Δ_i is inter-storey drift of the i^{th} floor.

The overall stiffness degradation curve and the inter-storey stiffness degradation curve are illustrated in Figures 14 and 15, respectively. As shown in Figures 14 and 15, it is revealed that:

- The overall converted stiffness decreases dramatically in the early test stage. The initial stiffness of the structure is 4.786 kN/mm. However, after main cracks appearing, the stiffness reduces to 71% of the initial value. With the cracking of concrete and the development of the inelastic deformation of the structure, the overall converted stiffness degradation slows down, and no abrupt changes are observed throughout the shaking table tests.
- The inter-storey stiffness of the 5th floor degrades slower than that of the 1st and 2nd floor during earthquake test runs, and the damage of the RAC frame beams and columns in the 1st and 2nd floor is more serious than other floors.
- Except the 5th floor, the degradation tendencies of the inter-storey stiffness from the 1st to 4th floor under different test phases are very close to each other.

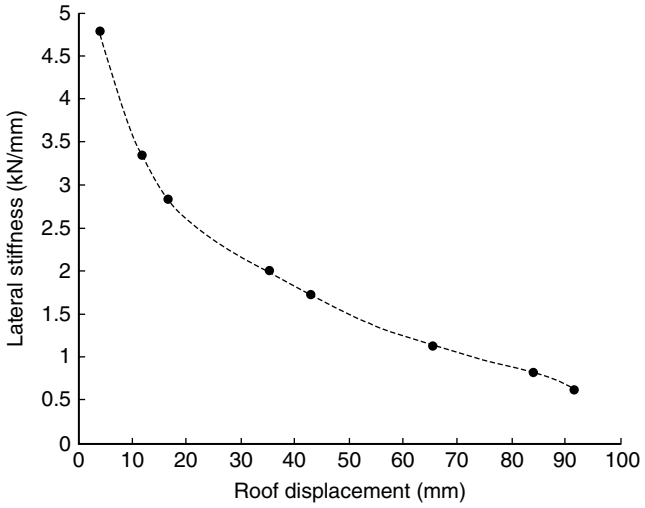

Figure 14. Overall stiffness degradation

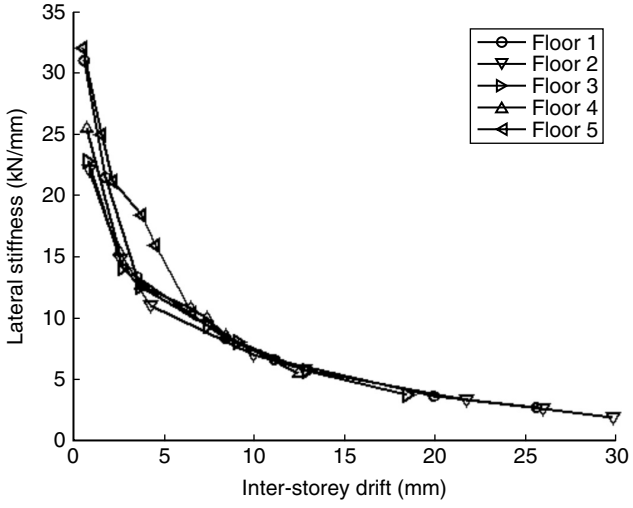

Figure 15. Inter-storey stiffness degradation

6. CONCLUSION

Based on the intensive analysis of hysteresis behavior of a cast-in-situ RAC frame structure tested on a shaking table, the following conclusions are derived.

(1) According to the test results, the hysteresis curves of the structure are obtained and studied. It reveals that the hysteresis behavior of the RAC frame structure is similar to that of the natural aggregate concrete (NAC) frame structure.

(2) From the skeleton fitting curve, the cracking load point, the yield load point, and the maximum load point are easily recognized, as well as the ultimate load point. The base shear-roof displacement skeleton curve reflects the variation of the lateral bearing capacity of the structure, and the slope of the curve represents the overall lateral stiffness of the structure.

(3) Based on the hysteresis curves obtained from shaking table tests, the feature point parameters of the skeleton curve and the stiffness degradation of the RAC frame model, a deteriorating four-line-typed restoring force model is put forward.

(4) In this hysteresis model the monotonic behavior is described by a four-line-typed skeleton curve which accounts for cracking of concrete, yielding of steel rebars, maximum loading point and ultimate loading point of the RAC frame model. The hysteresis behavior is described through a number of rules for unloading and reloading which are based on experimental data obtained from the tested model during earthquake test runs. Thus, the deteriorating four-line-typed restoring force model proposed can capture the hysteresis behavior of the structure at different nonlinear stages.

(5) The converted stiffness calculation formulae are defined and expressed according to Eqns 14 and 15. The overall converted stiffness

decreases dramatically in the early test stage. The initial stiffness of the structure is 4.786 kN/mm. However, after main cracks' appearing, the stiffness reduces to 71% of the initial value. With developing of concrete cracks and non-elastic deformation of the structure, the overall converted stiffness degradation slows down, and no abrupt changes are observed throughout the shaking table tests.

(6) The average roof displacement ductility factor calculated is 3.318, which demonstrates that the RAC frame model structure meets general structural seismic requirements if it is properly designed. The cast-in-situ RAC structure and the NAC structure have very similar displacement ductility and deformation capacity.

ACKNOWLEDGEMENTS

The authors wish to express appreciations to the National Natural Science Foundation of PR China (51325802), and the Science and Technology Commission of Shanghai (Grant No. 14231201300).

REFERENCES

Ajdukiewicz, A.B. and Kliszczewicz, A.T. (2007). "Comparative tests of beams and columns made of recycled aggregate concrete and natural aggregate concrete", *Journal of Advanced Concrete Technology*, Vol. 5, No. 2, pp. 259–273.

Cao, W.L., Yin, H.P., Zhang, J.W., Dong, H.Y. and Zhang, Y.Q. (2011). "Seismic behavior experiment of recycled concrete frame structures", *Journal of Beijing University of Technology*, Vol. 37, No. 2, pp. 191-198. (in Chinese)

Clough, R.W. (1966). *Effect of Stiffness Degradation on Earthquake Ductility Requirements*, Structural and Materials Research, Structural Engineering Laboratory, University of California, Berkeley, California, USA.

Corinaldesi, V. and Moriconi, G. (2006). "Behavior of beam-column joints made of sustainable concrete under cyclic loading", *Journal of Materials in Civil Engineering*, ASCE, Vol. 18, No. 5, pp. 650–658.

Etxeberria, M., Mari, A.R. and Vazquez, E. (2007). "Recycled aggregate concrete as structural material", *Materials and Structures*, Vol. 40, No. 5, pp. 529–541.

Fathifazl, G., Razaqpur, A.G., Isgor, O.B., Abbas, A., Fournier, B. and Foo, S. (2009). "Flexural performance of steel-reinforced recycled concrete beams", *ACI Structural Journal*, Vol. 106, No. 6, pp. 858–867.

Fathifazl, G., Razaqpu, A.G. and Isgor, O.B. (2010). "Shear strength of reinforced recycled concrete beams with stirrups", *Magazine of Concrete Research*, Vol. 62, No. 10, pp. 685–699.

Fukada, Y. (1969). "Study on the restoring force characteristics of reinforced concrete buildings", *Kanto District Symposium*, Architectural Institute of Japan, Tokyo, Japan. (in Japanese)

GB 50010. (2010). *Code for Design of Concrete Structures*, Chinese Building Press, Beijing, China. (in Chinese)

GB 50011. (2010). *Code for Seismic Design of Buildings*, Chinese Building Press, Beijing, China. (in Chinese)

Han, B.C., Yun, H.D and Chung, S.Y. (2001). "Shear capacity of reinforced concrete beams made with recycled aggregate", *ACI Special Publication*, Vol. 200, pp. 503–516.

Joseph, M.B., Andrei, M.R. and John, B.M. (1995). "Seismic resistance of reinforced concrete frame structures designed for gravity loads: Performance of structural system", *ACI Structural Journal*, Vol. 92, No. 5, pp. 597–609.

Liu, J.J., Lu, Z.T. and Feng, J. (2002). "Frame model with specially shape columns and transfer storey", *Journal of Building Structures*, Vol. 23, No. 1, pp. 21–26. (in Chinese)

Liu, Q., Xiao, J.Z. and Sun, Z. (2011). "Experimental study on the failure process of recycled concrete", *Cement and Concrete Research*, Vol. 41, No. 10, pp. 1050–1057.

Lu, X.L., Zhou, Y. and Yan, F. (2008). "Shaking table test and numerical analysis of RC frames with viscous wall dampers", *Journal of Structural Engineering*, ASCE, Vol. 134, No. 1, pp. 64–76.

Min, Z., Sun, W.M. and Guo, Z.G. (2011). "Experimental research on seismic behavior of recycled concrete frames", *World Earthquake Engineering*, Vol. 27, No. 1, pp. 22–27. (in Chinese)

Park, R. and Paulay, T. (1975). *Reinforced Concrete Structures*, John Wiley & Sons, New York, USA.

Takeda, T., Sozen, M.A. and Neilsen, N.N. (1970). "Reinforced concrete response to simulated earthquakes", *Journal of the Structural Division*, ASCE, Vol. 96, No. 12, pp. 2557–2573.

Tomazevic, M., Lutman, M. and Petkovic, L. (1996a). "Seismic behavior of masonry walls: experimental simulation", *Journal of Structural Engineering*, ASCE, Vol. 122, No. 9, pp. 1040–1047.

Tomazevic, M. and Lutman, M. (1996b). "Seismic behavior of masonry walls: modeling of hysteretic rules", *Journal of Structural Engineering*, ASCE, Vol. 122, No. 9, pp. 1048-1054.

Xiao, J.Z., Sun, Y.D. and Falkner, H. (2006). "Seismic performance of frame structures with recycled aggregate concrete", *Engineering Structures*, Vol. 28, No. 1, pp. 1–8.

Xiao, J.Z., Tawana, M.M. and Zhu, X.H. (2010). "Study on recycled aggregate concrete frame joints with method of nonlinear finite element", *Key Engineering Materials*, Vol. 417, pp. 745-748.

Xiao, J.Z., Li, J. and Chen, J. (2011). "Experimental study on the seismic response of braced reinforced concrete frame with irregular columns", *Earthquake Engineering and Engineering Vibration*, Vol. 10, No. 3, pp. 487–494.

Xiao, J.Z., Li, W.G., Fan, Y.H. and Huang, X. (2012a). "An overview of study on recycled aggregate concrete in China (1996-2011)", *Construction and Building Materials*, Vol. 31, pp. 364–383.

Xiao, J.Z., Wang, C.Q., Li, J. and Tawana, M.M. (2012b). "Shaking table model tests on recycled aggregate concrete frame structure", *ACI Structural Journal*, Vol. 109, No. 6, pp. 777–786.

Zhang, X.P. (2001). "Nonlinear analysis on reinforced concrete seismic structures", *Science Press*, Beijing, China. (in Chinese)

NOTATION

RCA	recycled coarse aggregate
RAC	recycled aggregate concrete
NAC	natural aggregate concrete
PGA	peak ground acceleration
V	the base shear
$\Delta(\Delta_i)$	the roof displacement (inter-storey drift)
P_c	the cracking load
P_y	the yield load
P_m	the maximum load
P_u	the ultimate load
Δ_c	the cracking displacement
Δ_y	the yield displacement
Δ_m	the maximum load
Δ_u	the ultimate displacement
μ	the ductility factor
β	the stiffness degradation factor